ACS OMEGA

Article

Cite This: ACS Omega XXXX, XXX, XXX−XXX

http://pubs.acs.org/journal/acsodf

Effects of Annealing Temperature and Ambient on Metal/$PtSe_2$ Contact Alloy Formation

Gioele Mirabelli,*[,†] Lee A. Walsh,[†] Farzan Gity,[†] Shubhadeep Bhattacharjee,[†] Conor P. Cullen,[§] Cormac Ó Coileáin,[§] Scott Monaghan,[†] Niall McEvoy,[§] Roger Nagle,[†] Paul K. Hurley,[†,‡] and Ray Duffy[†]

[†]Tyndall National Institute, University College Cork, Cork T12 R5CP, Ireland

[‡]School of Chemistry, University College Cork, Cork T12 K8AF, Ireland

[§]School of Chemistry, AMBER and CRANN, Trinity College Dublin, Dublin 2, Ireland

Supporting Information

ABSTRACT: Forming gas annealing is a common process step used to improve the performance of devices based on transition-metal dichalcogenides (TMDs). Here, the impact of forming gas anneal is investigated for $PtSe_2$-based devices. A range of annealing temperatures (150, 250, and 350 °C) were used both in inert (0/100% H_2/N_2) and forming gas (5/95% H_2/N_2) environments to separate the contribution of temperature and ambient. The samples are electrically characterized by circular transfer length method structures, from which contact resistance and sheet resistance are analyzed. Ti and Ni are used as metal contacts. Ti does not react with $PtSe_2$ at any given annealing step. In contrast to this, Ni reacts with $PtSe_2$, resulting in a contact alloy formation. The results are supported by a combination of X-ray photoelectron spectroscopy, Raman spectroscopy, energy-dispersive X-ray spectroscopy, and cross-sectional transmission electron microscopy. The work sheds light on the impact of forming gas annealing on TMD−metal interfaces, and on the TMD film itself, which could be of great interest to improve the contact resistance of TMD-based devices.

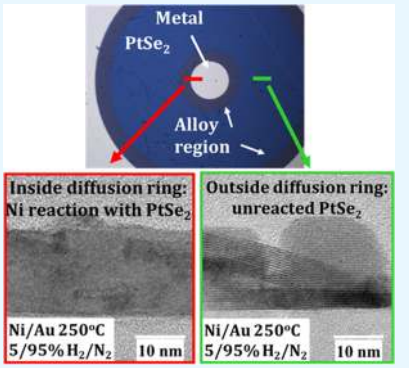

INTRODUCTION

Transition-metal dichalcogenides (TMDs) have been one of the most studied class of two-dimensional (2D) materials to date. Although promising, their integration with modern electronics is still limited due to the rather large Schottky barrier that usually characterizes the metal−TMD interface, which limits the device behavior, hiding their potential. In addition, most of the results are based on exfoliated flakes,[1,2] which causes a high variation from experiment to experiment, especially at low thickness. The lowest values of contact resistance are usually related to high-k induced doping[3,4] or interface engineering.[5−8] Although promising, another possible solution still mostly unexplored is the use of an opportune annealing step to modify the metal−TMD interface. Annealing is a common process step in the modern semiconductor industry. Laser annealing is used for Si and Ge to achieve highly doped and abrupt junctions.[9] Additionally, annealing in forming gas (FG) has been used to reduce fixed oxide charges and interface states at the Al_2O_3/InGaAs interface.[10] Similarly, for 2D-semiconductors, several publications have shown how different annealing steps can improve the performances of TMD-based devices. Vacuum annealing has been shown to reduce the concentration of surface contaminants.[11,12] Furthermore, annealing in an inert environment or FG can be beneficial in terms of reducing the density of interface states at the MoS_2/oxide interface.[13] Annealing steps have also been shown to be valuable for the TMD−metal interface. FG annealing (FGA) on graphene/MoS_2 contacts was shown to improve the contact resistance of the material.[14] Other annealing techniques, such as vacuum annealing,[15] microwave annealing,[16] or short-term pulsed annealing,[17] were also reported to be advantageous for the metal/MoS_2 interface. Nonetheless, the values are still far from the requirement of the International Roadmap for Semiconductors and Systems,[18] and the reaction metal−TMD upon annealing as well as the optimal annealing temperature range and ambient is still unclear.

In this work, we systematically characterize large-area grown thin films of $PtSe_2$ considering different postgrowth thermal treatments and their effects on the metal−TMD interface. $PtSe_2$ has attracted increasing interest over the last few years. As other TMDs, a monolayer of $PtSe_2$ is formed by a three-atom thick atomic cell, with the transition metal sandwiched between two chalcogen layers. Most TMDs show semiconductive properties, but interestingly, $PtSe_2$ shows semimetallic characteristics in its bulk form, whereas experiments have shown the opening of a band-gap for thicknesses lower than 3 nm, with ∼1.2 eV for a monolayer.[19,20] Therefore, $PtSe_2$

Received: July 23, 2019
Accepted: August 30, 2019

DOI: 10.1021/acsomega.9b02291
ACS Omega XXXX, XXX, XXX−XXX

has gained attention due to its potential application in electronics,[21] optoelectronics,[22] and sensors.[23] $PtSe_2$ can be uniformly grown over a large area by thermally assisted conversion (TAC), which does not require a high thermal budget (max temperature of 400 °C). This makes the growth compatible with back-end-of-line processing and integration in modern technologies, as it respects the typical thermal budgets of the CMOS industry (~450 °C).[24−26] This is in sharp contrast with TMD films grown by chemical vapor deposition, chemical vapor transport, or molecular beam epitaxy.[27−30] The growth is not homogenous, and it is characterized mainly by triangular crystals that merge together after a sufficient growth time.[31−33] Above this, the thermal budget of these processes is usually high to obtain a reaction of the predeposited film with the chalcogen, limiting their integration in modern CMOS technology.

The $PtSe_2$ was grown at 400 °C over a large area. Ti/Au and Ni/Au were used as metal contacts and circular transfer length method (c-TLM) structures were used to electrically characterize the metal/$PtSe_2$ interface and the $PtSe_2$ material itself. The samples were then annealed for 1 h in a FG ambient (5/95% H_2/N_2) at different annealing temperatures: 150, 250, and 350 °C. The same experiment was repeated in an inert environment (0/100% H_2/N_2). The electrical properties of the material were studied after each annealing step. The TMD−metal interface and alloy formation were studied and characterized by a combination of X-ray photoelectron spectroscopy (XPS), Raman spectroscopy, energy-dispersive X-ray (EDX) spectroscopy, and cross-sectional transmission electron microscopy (XTEM).

RESULTS

Figure 1 shows the process flow adopted to study the reaction of $PtSe_2$ after each annealing step. First, $PtSe_2$ (6−10 nm, with

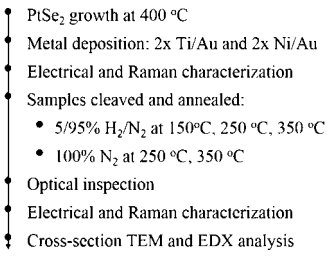

Figure 1. Experimental steps taken during this work.

an initial Pt thickness of 1 nm) was grown on four different samples in a single growth run for high consistency using a TAC process.[34] Because of this, applying a similar FGA step allows the effect of the process on the material itself and the metal−TMD interface to be decoupled. c-TLM structures were patterned by standard photolithography, and Ti/Au or Ni/Au were deposited by metal evaporation. Then, samples were measured electrically. The presence of $PtSe_2$ was confirmed by Raman analysis.

Figure 2a,d shows the optical microscope images of the contacted $PtSe_2$ with Ti and Ni contacts, respectively, before any annealing and no visible differences are present between the two samples. The samples then underwent different annealing steps. No obvious differences were found for the samples annealed in FG at 150 °C, as the temperature might have been too low to start any reactions. After annealing at 250 °C in forming or inert environment, the Ti/Au sample did not

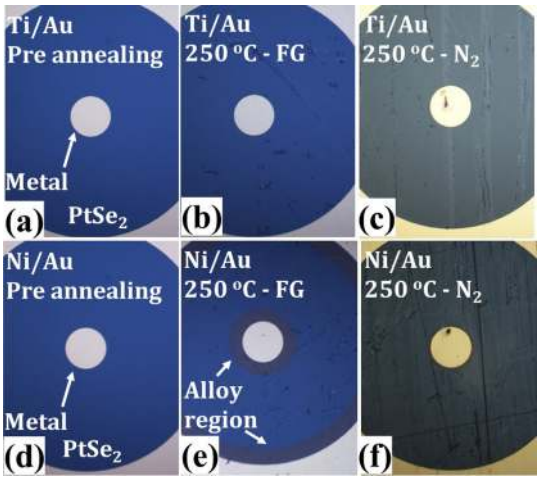

Figure 2. Optical microscope pictures of the larger c-TLM of $PtSe_2$ before annealing contacted with (a) Ti/Au and (d) Ni/Au. Same optical pictures repeated after annealing in FG and inert ambient at 250 °C for (b,c) Ti/Au and (e,f) Ni/Au, respectively. The darker gold ring in (e) clearly shows the alloy region.

show any appreciable differences from optical inspection (Figure 2b,c). In contrast, the Ni/Au sample annealed at 250 °C in FG displayed what looks like an "alloy region" around the metal contacts (Figure 2e). This alloy region is less pronounced for the annealing at the same temperature in the inert environment (Figure 2f). It is noted that the reaction taking place between Ni and $PtSe_2$ is accelerated by the presence of hydrogen during the annealing. The 350 °C anneal in FG (pictures not shown), as later confirmed by electrical and Raman characterizations, resulted in a degradation of the $PtSe_2$. Considering that $PtSe_2$ is grown at a temperature of 400 °C, a FG anneal at 350 °C may be too harsh an environment for this material, which highlights the importance of understanding the process window for optimal annealing temperature and its effects on the material properties.

Figure 3 shows the electrical characterization carried out on each sample. Figure 3a shows representative current−voltage measurements on the Ni/Au samples considering a spacing of 43.5 μm. Although no appreciable differences are visible from optical inspection after a FG anneal at 150 °C, the current decreases with respect to the pre-annealed case. In contrast, considering the same FG environment but a temperature of 250 °C, the current increases, meaning that the reaction that took place positively changed the metal/$PtSe_2$ interface. The difference is not related to a change in the properties of the channel as the annealing steps for the Ti/Au samples did not result in a change of the metal/$PtSe_2$ or the channel properties (Figure 3c). Consider that the results at 250 °C in FG were corrected because of the alloy region because it changed the spacing of each structure (the actual channel length). The anneal at 250 °C in an inert environment, similarly to the 150 °C in FG, resulted in a lower current. These two anneal conditions seem to provide similar results. Although, one was done at a lower temperature, the presence of FG seems to have accelerated the reactions that took place. It is also important to consider that the 250 °C in the inert environment also resulted in an alloy region, although not as pronounced as the case in FG. In contrast, no alloy regions were found for the sample annealed at 150 °C in FG.

DOI: 10.1021/acsomega.9b02291
ACS Omega XXXX, XXX, XXX−XXX

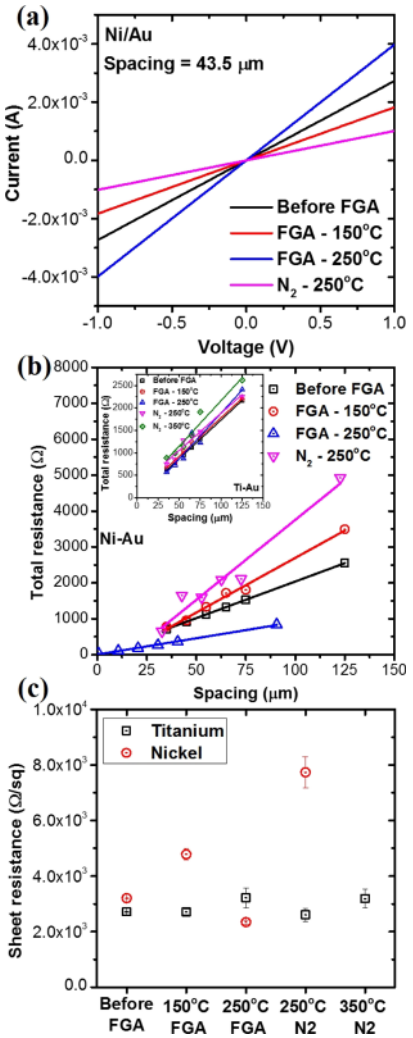

Figure 3. (a) Current−voltage measurements on the Ni/Au samples after each annealing step. (b) Total resistance vs spacing for the Ni/Au-contacted $PtSe_2$. Inset: total resistance vs spacing for the Ti/Au-contacted $PtSe_2$. (c) Extracted sheet resistance after each annealing step.

Figure 3b shows the total resistance versus spacing for the Ni/Au contacted $PtSe_2$ at each annealing step. It is clear that each annealing is affecting the electrical behavior of the device. Nonetheless, this analysis is problematic for the Ni/Au samples. Because of the presence of the alloy region, the fitting process is less reliable because the spacing of the structures change with the annealing condition. Future work may include linear TLMs with smaller dimensions for a more accurate parameter extraction. The inset of Figure 3b shows the same analysis for the Ti/Au sample for each annealing condition. No appreciable differences are present, and the trend remains quite similar, meaning that the film itself, as well as the $PtSe_2$/Ti interface, are not affected by any annealing steps.

Figure 3c shows the sheet resistance extracted from each measurement. The sheet resistance can be extracted from the Ti/Au measurements, considering the c-TLM theory.[35] However, for the Ni/Au samples, the total resistance was considered as the resistance of the $PtSe_2$ owing to the low contact resistance. The results for the Ti/Au contacts confirm what is seen in Figure 3a−c and from XTEM images (Figure S1): the annealing temperature and conditions are not changing the metal/$PtSe_2$ interface or the $PtSe_2$ material itself. In contrast, a much higher variation is seen for the Ni/Au samples, which can be related to the reaction between Ni and $PtSe_2$. Consider that, although obvious "alloy regions" are present from optical inspection it is possible that the Ni diffuses much further into the $PtSe_2$, than what is possible to see with an optical microscope.

Raman spectroscopy was then performed to confirm the integrity of the $PtSe_2$ and to probe the "alloy region" seen in the Ni/Au samples. The results are summarized in Table 1 (all Raman results are reported in Figure S2). In particular, the Raman signal was collected on the bare $PtSe_2$ and near the metal contact. For the Ti/Au sample, the signal of $PtSe_2$ is always present, except for the 350 °C annealing in FG, which resulted in degradation of the $PtSe_2$ film. Similarly, for the Ni/Au sample a clear $PtSe_2$ signal is present up to 250 °C, in both forming and inert gas environment in the bare $PtSe_2$ regions (far from the metal contact). For the samples that showed an "alloy region", no $PtSe_2$ signal is present close to the metal contact, suggesting metal interdiffusion and alloying.

Table 1. Summary of the Raman Analysis on the $PtSe_2$ Samples after Each Annealing Condition

	Raman peaks of $PtSe_2$	
annealing condition	Ti/Au	Ni/Au
150 °C 5/95% H_2/N_2	present	present
250 °C 5/95% H_2/N_2	present	present, except in diffusion ring
350 °C 5/95% H_2/N_2	absent	absent
250 °C 100% N_2	present	present
350 °C 100% N_2	present	absent

Figure 4 shows representative TEM images of the Ni/Au-contacted $PtSe_2$ samples annealed at 250 °C in FG and in an inert environment. Figure 4a,b compare the $PtSe_2$ structure inside and outside of the alloy region, respectively. It is noted that the layered structure is present outside the alloy region, whereas it is not inside it. Similarly, Figure 4c,d show the $PtSe_2$ below the metal contact and outside of it, respectively. Again, the layered structure is not present below the metal contact but is preserved outside of it. These representative images confirm the hypothesis. The diffusion ring seen from optical images is a result of Ni interdiffusing and alloying with the $PtSe_2$. This compound is not characterized by the same layered structure of $PtSe_2$, but it has the form of a 3D alloy. Also, although the alloy region around the contact is not present in the sample annealed at 250 °C in an inert environment, a similar reaction has taken place below the metal contact. Therefore, it can be concluded that the presence of hydrogen accelerates the reaction, and the Ni can react more readily with $PtSe_2$ away from the metal itself. It is also important to consider that defects as grain boundaries, steps or vacancies, are likely to lead to an increased activity compared to a defect-free film. These likely played a role in the process, considering both the polycrystalline nature of this film (Figure 4b) and the nanometer sized grain previously reported.[23]

In order to explore the nature of the interdiffusional alloying observed, XPS was performed using near-identical samples. Figure 5 shows XPS spectra of the Pt 4f and Se 3d core levels of $PtSe_2$ before and after metal deposition, with no further annealing. No Au was used here as Au does not interface with the $PtSe_2$. The Pt 4f spectra for bare $PtSe_2$ (Figure 5a) shows

DOI: 10.1021/acsomega.9b02291
ACS Omega XXXX, XXX, XXX−XXX

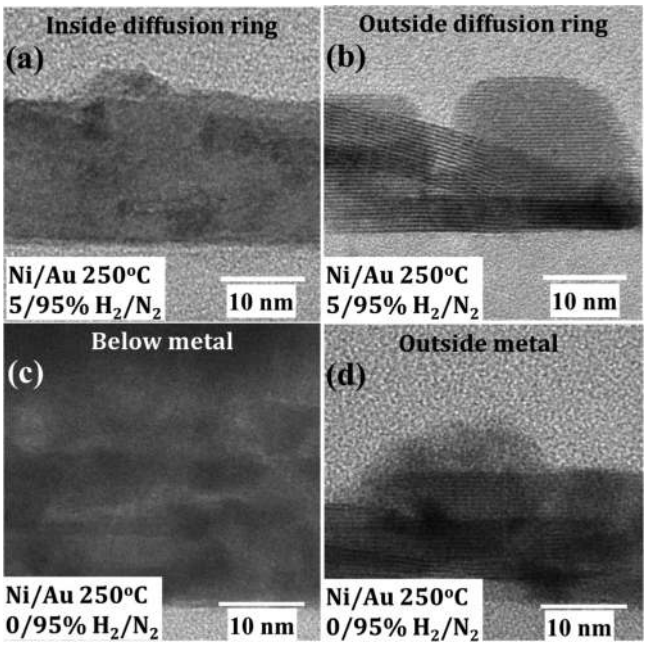

Figure 4. Representative XTEM images of the $PtSe_2$ contacted with Ni/Au. (a,b) show $PtSe_2$ after annealing in FG at 250 °C inside and outside the diffusion ring, respectively. (c,d) show the $PtSe_2$ after annealing in inert environment at 250 °C below the metal contact and outside the metal contact, respectively.

the presence of two chemical states, both represented by a doublet, one related to $PtSe_2$ (72.15 eV) and another due to surface oxidation (PtO_x at 71.1 eV). The Se 3d spectra of the same sample (Figure 5c) show $PtSe_2$ and SeO_x features (53.55 and 54.25 eV, respectively), with the additional contribution of the Pt $5p_{3/2}$ (52.6 eV), which overlaps with the Se 3d.

Upon Ni deposition, a significant change in the peak shape of the Pt 4f is observed, with the emergence of a feature at low binding energy (BE). This peak is at lower BE than PtO_x, consistent with metallic Pt (Pt_0). The Se 3d spectrum shows a subtler change with broadening to higher BE, attributed to the possible formation of a Ni/Se compound ($NiSe_x$). The Ni 2p spectra are difficult to interpret due to the presence of several satellite features. Although a change in line shape is observed in comparison to a reference Ni film, which could be due to Ni-oxidation or the reaction between Ni and a high electronegativity element such as Se. Additionally, the shift to higher BE may be due to charge transfer between the high work function Ni and $PtSe_2$. The Ni 2p spectra and further discussion can be found in the Supporting Information. Taken together this suggests the reduction of $PtSe_2$ by Ni, resulting in $NiSe_x$ formation and Pt metal.

In the case of Ti, a much more subtle change in chemical state is observed. After Ti deposition, the PtO_x peak increases significantly and is accompanied by a higher BE feature consistent with PtO_2. The Se 3d also shows a significant increase in oxidation with an increase in SeO_x and the appearance of a higher BE SeO_2 peak. The Ti 2p spectra (not shown) show the complete conversion of Ti to TiO_2, which is expected due to the oxygen-gettering nature of Ti. The presence of excess oxygen in the TiO_2 film in turn oxidizes the underlying $PtSe_2$.

Last, to confirm the presence of Ni in the reacted region, EDX was conducted on the TEM cross-section lamellas prepared with the Ni/Au-contacted devices before and after annealing at 250 °C in both FG and inert environment at 250 °C. Figure 6 shows the compositional analysis performed via scanning TEM (STEM)-based EDX spectroscopy. Figure 6a,f shows the high-angle annular dark-field (HAADF) images of the region under study, which is at the edge of the metal contact. Figure 6b–d,g–j show the spectra for Au, Pt, and Se. No significant interdiffusion is observed for these elements after annealing, and the mapping results are fairly similar. Considering that Au and Pt have a similar atomic weight, what would seem to be diffusion of Pt in Au is actually just an artefact from the EDX. This is not an issue as the focus is on the behavior of Ni with $PtSe_2$. Figure 6e,f shows clear Ni diffusion upon annealing. Before annealing, the Ni spectra is clearly confined between the $PtSe_2$ and the Au region. Whereas after N_2 annealing, significant diffusion of Ni into the Au and

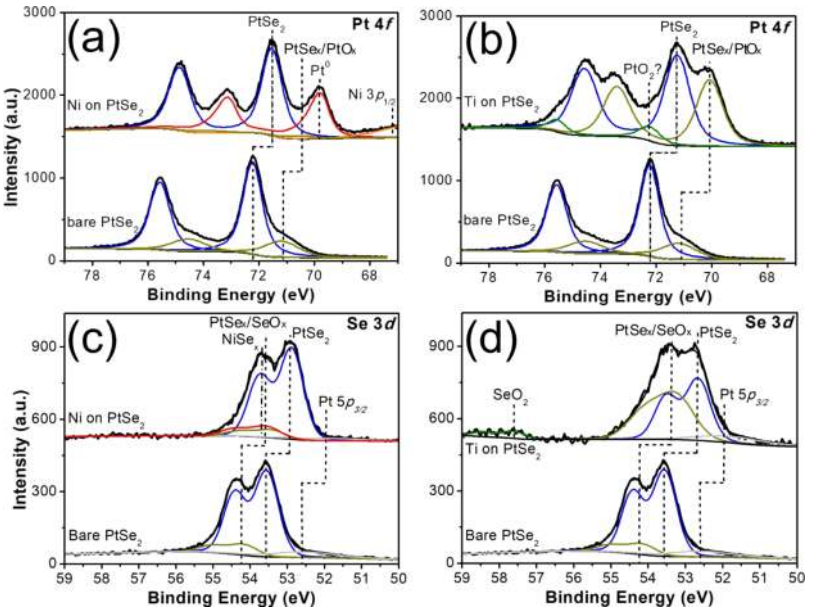

Figure 5. XPS spectra of (a,b) Pt 4f and (c,d) Se 3d core levels for $PtSe_2$ before and after Ni or Ti deposition.

DOI: 10.1021/acsomega.9b02291
ACS Omega XXXX, XXX, XXX−XXX

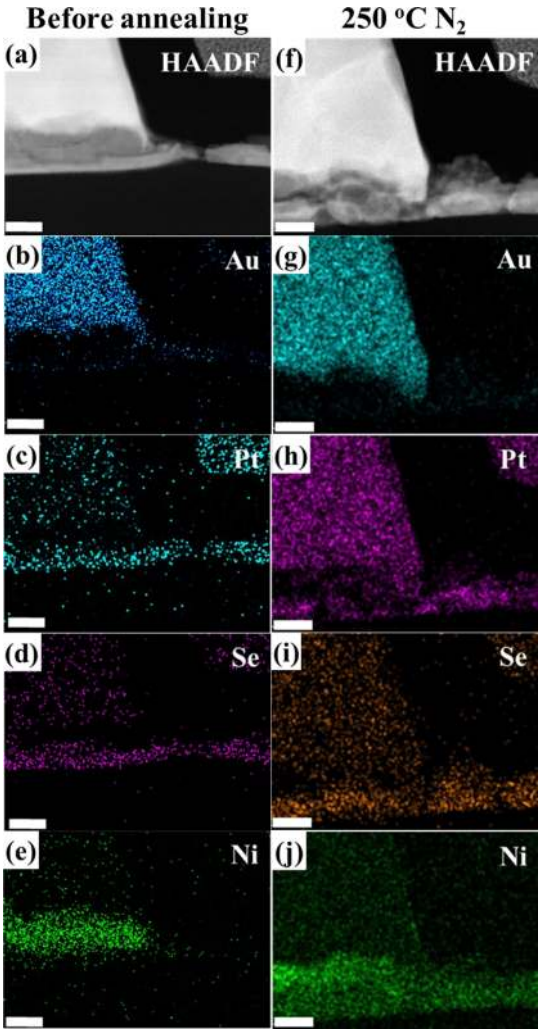

Figure 6. Compositional analysis performed via STEM-based EDX on Ni/Au-contacted $PtSe_2$ lamellas before and after annealing at 250 °C in N_2. (a,f) shows the HAADF image of the region under study before and after annealing respectively. (b–e) and (g–j) refer to the Au, Pt, Se, and Ni signal, before and after annealing, respectively. The scale bar is 25 nm.

$PtSe_2$ regions is observed. This is consistent with the diffusion seen in the optical images of c-TLM structures (Figure 2).

DISCUSSION

The interaction between top contacts and TMDs is significantly different to contacts on conventional semiconductors due to the van der Waals nature of the TMD surface. Density functional theory simulations predict that because of the lack of surface covalent bonds for most deposited metals, a van der Waals gap exists between the TMD surface and the metal contact.[36] This van der Waals gap acts as a tunnel barrier for carrier injection into the TMD channel, in addition to the Schottky barrier between the metal and TMD,[37] increasing total contact resistance.

A study by Das et al.[38] showed that the Schottky barriers between metals and MoS_2 are not consistent with the energy difference between the metal work function and the TMD Fermi level. They showed that even metals which would be expected to act as p-type contacts (i.e., Ni and Pt) instead exhibited electron injection consistent with n-type contacts. This was ascribed to Fermi level pinning in the MoS_2 close to the conduction band minimum at the metal/MoS_2 interface.[39]

Previous XPS studies on MoS_2 and WSe_2, considering a range of various metals,[40−43] have shown that similar reactions between the as-deposited metal and a TMD are possible. Nonetheless, an interface reaction does not necessarily result in a lower contact resistance because of the defective nature of exfoliated TMD flakes. However, a complete transformation of the TMD below the contact might mitigate the effect of contact resistance. Kappera et al.[7] demonstrated low contact resistance in a MoS_2 FET varying the phase of MoS_2 below the contact from semiconductive (2H) to metallic (1T). Similarly, here we showed a Ni/$PtSe_2$ alloy at the contact and $PtSe_2$ in the channel region. However, in this work, a contact resistance analysis was not possible. The $PtSe_2$ under study had a thickness of ∼6−10 nm, and in this thickness range, the $PtSe_2$ behaves as a semimetal, therefore it is not contact-resistance limited. Once the $PtSe_2$ growth processes are tuned further to achieve few-layer (<3 L) films, a more detailed contact resistance study could be performed. Also, the annealing temperature and ambient need to be optimized in order to control the diffusion/reaction of Ni.

A behavior similar to Ni and $PtSe_2$ has also been observed for Ag/MoS_2.[44] In that work, the samples were annealed between 250 and 350 °C in a rapid thermal annealing furnace for 300 s and the contact resistance values decreased after the thermal treatment because of Ag diffusion and doping below the contact regions. Although Ag does not react with MoS_2 at room temperature,[45] Souder and Brodie[46,47] showed that Ag diffused in bulk MoS_2 after annealing at 400−600 °C for 5 min, estimating a concentration of approximately 10^{19} cm^{-3}.

It is unclear if the Ni is acting as a dopant for $PtSe_2$, however, the metal−TMD reaction could be of great interest to improve the contact resistance of TMD-based devices.

CONCLUSIONS

In this study, the Ti/$PtSe_2$ and Ni/$PtSe_2$ interfaces were explored, along with the impact of post-metallization anneals in FG and inert ambient. Electrical and chemical characterization show that Ti is unreactive after annealing, even at relatively high temperature, whereas Ni readily reacts with $PtSe_2$ to form $NiSe_x$ and reduced $PtSe_x$/Pt/metal. The reaction is enhanced with high temperatures or a hydrogen-rich environment, which can cause the Ni to diffuse laterally into the $PtSe_2$. The metal/$PtSe_2$ alloying is a possible solution for reducing contact resistance in few-layer devices based on $PtSe_2$ and other TMD materials.

EXPERIMENTAL SECTION

Growth. All $PtSe_2$ samples were grown over large area. Pt metal evaporated onto a SiO_2/Si substrate. This was then converted in a furnace with a Se pressure of ∼1 mbar at 400 °C. The specifics of the growth are discussed in detail elsewhere.[48]

Metal Deposition. c-TLM metal contacts were patterned using standard photolithography followed by e-beam evaporation of the metal and a lift-off process. For these devices the targeted thicknesses were 10/90 nm for both Ti/Au and Ni/Au at a background pressure of $\sim 10^{-5}$ mbar. For the XPS samples, the targeted thicknesses were 3 nm for both Ti and Ni. No Au was used in the XPS samples as it does not interface with the $PtSe_2$ film and the added metal thickness would

DOI: 10.1021/acsomega.9b02291
ACS Omega XXXX, XXX, XXX−XXX

exceed the photoelectron escape depth (of ∼5 nm). After an initial characterization, each sample was cleaved into three pieces to maintain consistency. FG anneals were performed at 150, 250, and 350 °C for 1 h using 5% H_2/95% N_2. The same annealing conditions were applied again in an inert environment (0% H_2/100% N_2).

Characterization. XPS characterization was performed using monochromated Al Kα X-rays from an Omicron XM1000 MkII X-ray source and Omicron EA125 hemispherical analyzer with ±0.05 eV resolution. A take-off angle of 45°, acceptance angle of 8°, and pass energy of 15 eV were employed during spectral acquisition. The BE scale was referenced to the adventitious carbon species in the C 1s core level (285.8 eV). Spectra were deconvolved using AAnalyzer,[49] a curve fitting software.

For structural analysis, cross-section samples were obtained by using the Dual Beam Helios NanoLab 600i system from FEI, using a Ga ion beam. Layers of the protective material were used consisting of electron beam deposited C, Pt, and ion beam deposited C. Lamellas were thinned and polished at 30 kV 100 pA and 5 kV 47 pA, respectively. XTEM imaging was carried out using a JEOL 2100 HRTEM, operated at 200 kV in the bright field mode using a Gatan double tilt holder. EDX mapping was carried out using a Thermo Fisher Scientific Titan Themis operated of 300 kV in the STEM mode using the Bruker SuperX silicon drift detector.

■ ASSOCIATED CONTENT

Supporting Information

The Supporting Information is available free of charge on the ACS Publications website at DOI: 10.1021/acsomega.9b02291.

XTEM of Ti/Au-contacted $PtSe_2$, Raman analysis considering variation in annealing temperature and ambient, and additional XPS spectra of the Ni/$PtSe_2$ and Ti/$PtSe_2$ interface (PDF)

■ AUTHOR INFORMATION

Corresponding Author

*E-mail: gioele.mirabelli@tyndall.ie.

ORCID

Gioele Mirabelli: 0000-0001-7060-4836

Lee A. Walsh: 0000-0002-6688-8626

Farzan Gity: 0000-0003-3128-1426

Scott Monaghan: 0000-0002-9006-9890

Notes

The authors declare no competing financial interest.

■ ACKNOWLEDGMENTS

The authors would like to thank Alan Harvey for the EDX analysis. We also acknowledge the support of Science Foundation Ireland through the US-Ireland R&D Partnership Programme "Understanding the Nature of Interfaces in Two Dimensional Electronics (UNITE)" grant number SFI/13/US/I2862, the SFI project INVEST (15/IA/3131), and the support of the Irish Research Council through the Postgraduate Scholarship EPSPG/2015/69. The research was supported in part by the Higher Education Authority Programme for Research in Third Level Institutions in Ireland under grant agreement no. HEA PRTLI5. This work was also supported in part by the European Union's Horizon 2020 research and innovation program under the Marie Skłodowska-Curie grant agreement no. 713567 and a research grant from Science Foundation Ireland (SFI) under grant number SFI/12/RC/2278.

■ REFERENCES

(1) Novoselov, K. S.; Jiang, D.; Schedin, F.; Booth, T. J.; Khotkevich, V. V.; Morozov, S. V.; Geim, A. K. Two-dimensional atomic crystals. *Proc. Natl. Acad. Sci. U.S.A.* **2005**, *102*, 10451−10453.

(2) Radisavljevic, B.; Radenovic, A.; Brivio, J.; Giacometti, V.; Kis, A. Single-layer MoS2 transistors. *Nat. Nanotechnol.* **2011**, *6*, 147.

(3) Valsaraj, A.; Chang, J.; Rai, A.; Register, L. F.; Banerjee, S. K. Theoretical and experimental investigation of vacancy-based doping of monolayer MoS_2 on oxide. *2D Mater.* **2015**, *2*, 045009.

(4) Alharbi, A.; Shahrjerdi, D. Analyzing the Effect of High-k Dielectric-Mediated Doping on Contact Resistance in Top-Gated Monolayer MoS2 Transistors. *IEEE Trans. Electron Devices* **2018**, *65*, 4084−4092.

(5) Leong, W. S.; Luo, X.; Li, Y.; Khoo, K. H.; Quek, S. Y.; Thong, J. T. L. Low Resistance Metal Contacts to MoS_2 Devices with Nickel-Etched-Graphene Electrodes. *ACS Nano* **2015**, *9*, 869−877.

(6) Cui, X.; Shih, E.-M.; Jauregui, L. A.; Chae, S. H.; Kim, Y. D.; Li, B.; Seo, D.; Pistunova, K.; Yin, J.; Park, J.-H.; Choi, H.-J.; Lee, Y. H.; Watanabe, K.; Taniguchi, T.; Kim, P.; Dean, C. R.; Hone, J. C. Low-Temperature Ohmic Contact to Monolayer MoS_2 by van der Waals Bonded Co/h-BN Electrodes. *Nano Lett.* **2017**, *17*, 4781−4786.

(7) Kappera, R.; Voiry, D.; Yalcin, S. E.; Branch, B.; Gupta, G.; Mohite, A. D.; Chhowalla, M. Phase-engineered low-resistance contacts for ultrathin MoS_2 transistors. *Nat. Mater.* **2014**, *13*, 1128.

(8) Leong, W. S.; Ji, Q.; Mao, N.; Han, Y.; Wang, H.; Goodman, A. J.; Vignon, A.; Su, C.; Guo, Y.; Shen, P.-C.; Gao, Z.; Muller, D. A.; Tisdale, W. A.; Kong, J. Synthetic Lateral Metal-Semiconductor Heterostructures of Transition Metal Disulfides. *J. Am. Chem. Soc.* **2018**, *140*, 12354−12358.

(9) Cristiano, F.; Shayesteh, M.; Duffy, R.; Huet, K.; Mazzamuto, F.; Qiu, Y.; Quillec, M.; Henrichsen, H. H.; Nielsen, P. F.; Petersen, D. H.; La Magna, A.; Caruso, G.; Boninelli, S. Defect evolution and dopant activation in laser annealed Si and Ge. *Mater. Sci. Semicond. Process.* **2016**, *42*, 188−195.

(10) Hurley, P. K.; O'Connor, E.; Djara, V.; Monaghan, S.; Povey, I. M.; Long, R. D.; Sheehan, B.; Lin, J.; McIntyre, P. C.; Brennan, B.; Wallace, R. M.; Pemble, M. E.; Cherkaoui, K. The Characterization and Passivation of Fixed Oxide Charges and Interface States in the Al_2O_3/InGaAs MOS System. *IEEE Trans. Device Mater. Reliab.* **2013**, *13*, 429−443.

(11) Qiu, H.; Pan, L.; Yao, Z.; Li, J.; Shi, Y.; Wang, X. Electrical characterization of back-gated bi-layer MoS_2 field-effect transistors and the effect of ambient on their performances. *Appl. Phys. Lett.* **2012**, *100*, 123104.

(12) Kim, J. H.; Lee, J.; Kim, J. H.; Hwang, C. C.; Lee, C.; Park, J. Y. Work function variation of MoS_2 atomic layers grown with chemical vapor deposition: The effects of thickness and the adsorption of water/oxygen molecules. *Appl. Phys. Lett.* **2015**, *106*, 251606.

(13) Bolshakov, P.; Zhao, P.; Azcatl, A.; Hurley, P. K.; Wallace, R. M.; Young, C. D. Electrical characterization of top-gated molybdenum disulfide field-effect-transistors with high-k dielectrics. *Microelectron. Eng.* **2017**, *178*, 190−193.

(14) Lu, Q.; Fang, C.; Liu, Y.; Shao, Y.; Han, G.; Zhang, J.; Hao, Y. Temperature dependence of annealing on the contact resistance of MoS_2 with graphene electrodes observed. *Jpn. J. Appl. Phys.* **2018**, *57*, 04FP07.

(15) Baugher, B. W. H.; Churchill, H. O. H.; Yang, Y.; Jarillo-Herrero, P. Intrinsic Electronic Transport Properties of High-Quality Monolayer and Bilayer MoS_2. *Nano Lett.* **2013**, *13*, 4212−4216.

(16) Yang, H.; Li, C.; Yue, L.; Wen, C.; Zhang, J.; Wu, D. Improving Electrical Performance of Few-Layer MoS_2 FETs via Microwave Annealing. *IEEE Electron Device Lett.* **2019**, *40*, 1116−1119.

DOI: 10.1021/acsomega.9b02291
ACS Omega XXXX, XXX, XXX−XXX

(17) Kwon, H.-J.; Kim, S.; Jang, J.; Grigoropoulos, C. P. Evaluation of pulsed laser annealing for flexible multilayer MoS_2 transistors. *Appl. Phys. Lett.* **2015**, *106*, 113111.
(18) *International Roadmap for Devices and Systems IRDS*, 2017; https://irds.ieee.org/.
(19) Ciarrocchi, A.; Avsar, A.; Ovchinnikov, D.; Kis, A. Thickness-modulated metal-to-semiconductor transformation in a transition metal dichalcogenide. *Nat. Commun.* **2018**, *9*, 919.
(20) Wang, Y.; Li, L.; Yao, W.; Song, S.; Sun, J. T.; Pan, J.; Ren, X.; Li, C.; Okunishi, E.; Wang, Y.-Q.; Wang, E.; Shao, Y.; Zhang, Y. Y.; Yang, H.-t.; Schwier, E. F.; Iwasawa, H.; Shimada, K.; Taniguchi, M.; Cheng, Z.; Zhou, S.; Du, S.; Pennycook, S. J.; Pantelides, S. T.; Gao, H.-J. Monolayer $PtSe_2$, a New Semiconducting Transition-Metal-Dichalcogenide, Epitaxially Grown by Direct Selenization of Pt. *Nano Lett.* **2015**, *15*, 4013−4018.
(21) Yim, C.; Passi, V.; Lemme, M. C.; Duesberg, G. S.; Ó Coileáin, C.; Pallecchi, E.; Fadil, D.; McEvoy, N. Electrical devices from top-down structured platinum diselenide films. *npj 2D Mater. Appl.* **2018**, *2*, 5.
(22) Yim, C.; McEvoy, N.; Riazimehr, S.; Schneider, D. S.; Gity, F.; Monaghan, S.; Hurley, P. K.; Lemme, M. C.; Duesberg, G. S. Wide Spectral Photoresponse of Layered Platinum Diselenide-Based Photodiodes. *Nano Lett.* **2018**, *18*, 1794−1800.
(23) Wagner, S.; Yim, C.; McEvoy, N.; Kataria, S.; Yokaribas, V.; Kuc, A.; Pindl, S.; Fritzen, C.-P.; Heine, T.; Duesberg, G. S.; Lemme, M. C. Highly Sensitive Electromechanical Piezoresistive Pressure Sensors Based on Large-Area Layered $PtSe_2$ Films. *Nano Lett.* **2018**, *18*, 3738−3745.
(24) Sedky, S.; Witvrouw, A.; Bender, H.; Baert, K. Experimental determination of the maximum post-process annealing temperature for standard CMOS wafers. *IEEE Trans. Electron Devices* **2001**, *48*, 377−385.
(25) Takeuchi, H.; Wung, A.; Sun, X.; Howe, R. T.; King, T.-J. Thermal budget limits of quarter-micrometer foundry CMOS for post-processing MEMS devices. *IEEE Trans. Electron Devices* **2005**, *52*, 2081−2086.
(26) Lee, Y. H. D.; Lipson, M. Back-End Deposited Silicon Photonics for Monolithic Integration on CMOS. *IEEE J. Sel. Top. Quantum Electron.* **2013**, *19*, 8200207.
(27) Hu, D.; Xu, G.; Xing, L.; Yan, X.; Wang, J.; Zheng, J.; Lu, Z.; Wang, P.; Pan, X.; Jiao, L. Two-Dimensional Semiconductors Grown by Chemical Vapor Transport. *Angew. Chem., Int. Ed.* **2017**, *56*, 3611−3615.
(28) Mleczko, M. J.; Xu, R. L.; Okabe, K.; Kuo, H.-H.; Fisher, I. R.; Wong, H.-S. P.; Nishi, Y.; Pop, E. High Current Density and Low Thermal Conductivity of Atomically Thin Semimetallic WTe_2. *ACS Nano* **2016**, *10*, 7507−7514.
(29) Walsh, L. A.; Addou, R.; Wallace, R. M.; Hinkle, C. L. Molecular Beam Epitaxy of Transition Metal Dichalcogenides. In *Molecular Beam Epitaxy*, 2nd ed.; Henini, M., Ed.; Elsevier, 2018; Chapter 22, pp 515−531.
(30) Roy, A.; Movva, H. C. P.; Satpati, B.; Kim, K.; Dey, R.; Rai, A.; Pramanik, T.; Guchhait, S.; Tutuc, E.; Banerjee, S. K. Structural and Electrical Properties of $MoTe_2$ and $MoSe_2$ Grown by Molecular Beam Epitaxy. *ACS Appl. Mater. Interfaces* **2016**, *8*, 7396−7402.
(31) Xia, J.; Huang, X.; Liu, L.-Z.; Wang, M.; Wang, L.; Huang, B.; Zhu, D.-D.; Li, J.-J.; Gu, C.-Z.; Meng, X.-M. CVD synthesis of large-area, highly crystalline $MoSe_2$ atomic layers on diverse substrates and application to photodetectors. *Nanoscale* **2014**, *6*, 8949−8955.
(32) Schmidt, H.; Wang, S.; Chu, L.; Toh, M.; Kumar, R.; Zhao, W.; Castro Neto, A. H.; Martin, J.; Adam, S.; Özyilmaz, B.; Eda, G. Transport Properties of Monolayer MoS_2 Grown by Chemical Vapor Deposition. *Nano Lett.* **2014**, *14*, 1909−1913.
(33) Kang, K.; Xie, S.; Huang, L.; Han, Y.; Huang, P. Y.; Mak, K. F.; Kim, C.-J.; Muller, D.; Park, J. High-mobility three-atom-thick semiconducting films with wafer-scale homogeneity. *Nature* **2015**, *520*, 656.
(34) Yim, C.; Lee, K.; McEvoy, N.; O'Brien, M.; Riazimehr, S.; Berner, N. C.; Cullen, C. P.; Kotakoski, J.; Meyer, J. C.; Lemme, M. C.; Duesberg, G. S. High-Performance Hybrid Electronic Devices from Layered $PtSe_2$ Films Grown at Low Temperature. *ACS Nano* **2016**, *10*, 9550−9558.
(35) Klootwijk, J. H.; Timmering, C. E. In Merits and limitations of circular TLM structures for contact resistance determination for novel III-V HBTs. *Proceedings of the 2004 International Conference on Microelectronic Test Structures*; IEEE Cat. No. 04CH37516, March 22−25, 2004, 2004; pp 247−252.
(36) Kang, J.; Liu, W.; Sarkar, D.; Jena, D.; Banerjee, K. Computational Study of Metal Contacts to Monolayer Transition-Metal Dichalcogenide Semiconductors. *Phys. Rev. X* **2014**, *4*, 031005.
(37) Kwon, J.; Lee, J.-Y.; Yu, Y.-J.; Lee, C.-H.; Cui, X.; Hone, J.; Lee, G.-H. Thickness-dependent Schottky barrier height of MoS_2 field-effect transistors. *Nanoscale* **2017**, *9*, 6151−6157.
(38) Das, S.; Chen, H.-Y.; Penumatcha, A. V.; Appenzeller, J. High Performance Multilayer MoS_2 Transistors with Scandium Contacts. *Nano Lett.* **2013**, *13*, 100−105.
(39) Kim, C.; Moon, I.; Lee, D.; Choi, M. S.; Ahmed, F.; Nam, S.; Cho, Y.; Shin, H.-J.; Park, S.; Yoo, W. J. Fermi Level Pinning at Electrical Metal Contacts of Monolayer Molybdenum Dichalcogenides. *ACS Nano* **2017**, *11*, 1588−1596.
(40) McDonnell, S.; Smyth, C.; Hinkle, C. L.; Wallace, R. M. MoS_2−Titanium Contact Interface Reactions. *ACS Appl. Mater. Interfaces* **2016**, *8*, 8289−8294.
(41) Smyth, C. M.; Walsh, L. A.; Bolshakov, P.; Catalano, M.; Addou, R.; Wang, L.; Kim, J.; Kim, M. J.; Young, C. D.; Hinkle, C. L.; Wallace, R. M. Engineering the Palladium−WSe_2 Interface Chemistry for Field Effect Transistors with High-Performance Hole Contacts. *ACS Appl. Nano Mater.* **2019**, *2*, 75−88.
(42) Smyth, C. M.; Addou, R.; McDonnell, S.; Hinkle, C. L.; Wallace, R. M. WSe_2-contact metal interface chemistry and band alignment under high vacuum and ultra high vacuum deposition conditions. *2D Mater.* **2017**, *4*, 025084.
(43) Smyth, C. M.; Addou, R.; McDonnell, S.; Hinkle, C. L.; Wallace, R. M. Contact Metal−MoS_2 Interfacial Reactions and Potential Implications on MoS_2-Based Device Performance. *J. Phys. Chem. C* **2016**, *120*, 14719−14729.
(44) Abraham, M.; Mohney, S. E. Annealed Ag contacts to MoS_2 field-effect transistors. *J. Appl. Phys.* **2017**, *122*, 115306.
(45) Lince, J. R.; Carré, D. J.; Fleischauer, P. D. Schottky-barrier formation on a covalent semiconductor without Fermi-level pinning: The metal-MoS_2(0001) interface. *Phys. Rev. B: Condens. Matter Mater. Phys.* **1987**, *36*, 1647−1656.
(46) Souder, A. D.; Brodie, D. E. The Effect of Contact Annealing on Hall Data for MoS_2 Layer Structures. *Can. J. Phys.* **1972**, *50*, 1223−1225.
(47) Souder, A.; Brodie, D. E. Electrical Contacts and Conductivity of MoS_2 Layer Structures. *Can. J. Phys.* **1971**, *49*, 2565−2571.
(48) O'Brien, M.; McEvoy, N.; Motta, C.; Zheng, J.-Y.; Berner, N. C.; Kotakoski, J.; Elibol, K.; Pennycook, T. J.; Meyer, J. C.; Yim, C.; Abid, M.; Hallam, T.; Donegan, J. F.; Sanvito, S.; Duesberg, G. S. Raman characterization of platinum diselenide thin films. *2D Mater.* **2016**, *3*, 021004.
(49) Herrera-Gomez, A. *AAnalyzer*, 2002.

DOI: 10.1021/acsomega.9b02291
ACS Omega XXXX, XXX, XXX−XXX